Insights into characteristics and formation mechanisms of secondary organic aerosols in Guangzhou urban area

Miaomiao Zhai[1,3], Ye Kuang[1,3*], Li Liu[2,*], Yao He[1,3], Biao Luo[1,3], Wanyun Xu[4], Jiangchuan Tao[1,3], Yu Zou[2], Fei Li[2,5], Changqin Yin[2,7], Chunhui Li[2], Hanbing Xu[6], Xuejiao Deng[2]

[1] Institute for Environmental and Climate Research, Jinan University, Guangzhou, China.

[2] Key Laboratory of Regional Numerical Weather Prediction, Institute of Tropical and Marine Meteorology, China Meteorological Administration, Guangzhou, 510640，China

[3] Guangdong-Hongkong-Macau Joint Laboratory of Collaborative Innovation for Environmental Quality, Guangzhou, China.

[4] State Key Laboratory of Severe Weather & Key Laboratory for Atmospheric Chemistry, Institute of Atmospheric Composition, Chinese Academy of Meteorological Sciences, Beijing, 100081, China

[5] Xiamen Key Laboratory of Straits Meteorology, Xiamen Meteorological Bureau, Xiamen, 361012, China

[6] Experimental Teaching Center, Sun Yat-Sen University, Guangzhou 510275, China

[7] Shanghai Key Laboratory of Meteorology and Health, Shanghai Meteorological Bureau, Shanghai 200030, China

*Correspondence to: Ye Kuang (kuangye@jnu.edu.cn) and Li Liu (liul@gd121.cn)

38 **Abstract**

39   Emission controls have substantially brought down aerosol pollution in China, however, aerosol

40 mass reductions have slowed down in recent years in the Pearl River Delta (PRD) region, where

41 secondary organic aerosol (SOA) formation poses a major challenge for air quality improvement. In

42 this study, we characterized the roles of SOA in haze formation in urban Guangzhou City of the PRD

43 using year-long aerosol mass spectrometer measurements for the first time and discussed possible

44 pathways of SOA formations. On average, organic aerosols (OA) contribute dominantly (50%) to non-

45 refractory submicron aerosol mass ($NR\text{-}PM_1$). The average mass concentration of SOA (including by

46 less and more oxidized OA, LOOA and MOOA) contributed most to $NR\text{-}PM_1$, reaching about 1.7

47 times that of primary organic aerosols (POA, including hydrocarbon-like and cooking-related OA) and

48 accounting for 32% of $NR\text{-}PM_1$, even more than sulfate (22%) and nitrate (16%). Seasonal variations

49 of $NR\text{-}PM_1$ revealed that haze formation mechanisms differed much among distinct seasons. Sulfate

50 mattered more than nitrate in fall, while nitrate was more important than sulfate in spring and winter,

51 with SOA contributing significantly to haze formations in all seasons. Daytime SOA formation was

52 weak in winter under low oxidant level and air relative humidity, whereas prominent daytime SOA

53 formation was observed in fall, spring and summer almost on daily basis, suggesting for important

54 roles of photochemistry in SOA formations. Further analysis showed that the coordination of gas-phase

55 photochemistry and subsequent aqueous-phase reactions likely played significant roles in quick

56 daytime SOA formations. Obvious nighttime SOA formations were also frequently observed in spring,

57 fall and winter, and it was found that daytime and nighttime SOA formations together had resulted in

58 the highest SOA concentrations in these seasons and contributed substantially to severe haze

59 formations. Simultaneous increases of nitrate with SOA after sunset suggested the important roles of

60 NO_3 radical chemistry in nighttime SOA formations, and confirmed by continuous increase of

61 NO^+/NO_2^+ fragment ratio that related to measured particulate nitrate after sunset. Findings of this study

62 have promoted our understanding in haze pollution characteristics of the PRD and laid down future

63 directions on investigations of SOA formation mechanisms in urban areas of southern China that share

64 similar emission sources and meteorological conditions.

65

1 Introduction

Ubiquitous submicron aerosols in the atmosphere not only deteriorate human health and visibility, but also impact climate through interactions with solar radiation and clouds. Organic aerosols (OA) represent one of the most important and sometimes even dominant components (~10-90%) of PM_1 (aerosol particles with aerodynamic diameter less than 1 μm) in urban, rural and remote areas (Zhang et al., 2007;Jimenez et al., 2009). OA can either be emitted directly from emission sources or be formed through atmospheric reactions of volatile organic compounds, the former is referred to as primary OA (POA) and the latter is referred to as secondary OA (SOA). An increasing number of researches show that SOA account for a large fraction of OA worldwide (Zhang et al., 2007;Zhang et al., 2011), and even dominate in some cases (Kuang et al., 2020). The implementation of strict emission reduction policies has significantly improved the air quality of Pearl River Delta (PRD) region, which is a highly industrialized area of China, and the annual mean concentration of $PM_{2.5}$ (particulate matter with aerodynamic diameter less than 2.5 μm) has been brought down to less than 30 μg/m^3 (Xu et al., 2020). However, the reduction of $PM_{2.5}$ mass concentrations in PRD has slowed down substantially in recent years, which might be related to the significant increases in the proportion of secondary aerosols (Xu et al., 2020), especially for SOA. However, long-term observations that elucidate the sources and secondary formations of OA in this area is still missing.

Aerosol mass spectrometers are advanced on-line instruments that provide real time quantitative characterization of aerosol particle compositions (Jayne et al., 2000;Canagaratna et al., 2007;Jimenez et al., 2003). Positive matrix factorization (PMF) (Ulbrich et al., 2009) or a multilinear engine (ME-2) (Paatero, 1999;Canonaco et al., 2013) can be employed to further resolve different OA factors that are associated with different sources and formation mechanisms from the OA mass spectra. Although aerosol mass spectrometers have been widely used in China in recent years, most studies have been conducted in specific periods due to its high cost and maintenance (He et al., 2011;Chen et al., 2021;Qin et al., 2017), resulting in few long-term characterizations of the mass concentrations and chemical compositions of PM_1. The design of Aerosol Chemical Speciation Monitor (ACSM) has improved this problem to some extent (Ng et al., 2011;Sun et al., 2015). Based on 2-year ACSM measurements, Sun et al. (2018) investigate the distinct characteristics of PM_1 compositions among different seasons in Beijing urban area. Canonaco et al. (2021) also performed a long-term source

95 apportionment on a 1-year ACSM dataset from downtown Zurich. Many other studies also have

96 successfully applied the ACSM in the monitoring organic aerosols in various regions (Sun et al.,

97 2012;Sun et al., 2013;Sun et al., 2014;Sun et al., 2016;Fröhlich et al., 2013;Allan et al., 2010;Zhang et

98 al., 2012;Xu et al., 2015a;Zhou et al., 2020;Huang et al., 2014;Hu et al., 2016;Via et al., 2021), however

99 long-term measurements are still relatively scarce, and remain missing in urban areas of the PRD

100 region.

101 Guo et al. (2020) found that OA played a dominant role in PM_1 during winter in Guangzhou, a

102 mega city of the PRD, and the results of OA source apportionment emphasized the dominance of SOA.

103 Qin et al. (2017) and Huang et al. (2011) also reported similar results during autumn and winter in

104 Guangzhou. In fact, the compositions, sources, and evolution processes differ much among seasons

105 due to changes in emission sources and meteorological conditions (Li et al., 2015). Thus, long-term

106 characterizations that cover measurements of different seasons are urgently needed to gain insights

107 into emission sources and formation mechanisms of OA, thereby helping to address the challenge of

108 fine particulate matter pollution mitigation in the PRD region.

109 In this study, we performed a year-long continuous measurement of non-refractory submicron

110 aerosols ($NR-PM_1$) with an ACSM in urban Guangzhou from September 2020 to August 2021 to

111 characterize POA sources and investigate SOA formation mechanisms in different seasons.

2 Experimental methods

2.1 sampling site and measurements

114 A quadrupole-Aerosol Chemical Speciation Monitor (Q-ACSM) was deployed to continuously

115 measure nonrefractory PM_1 ($NR-PM_1$) species including OA, sulfate (SO_4), nitrate (NO_3), ammonium

116 (NH_4), and chloride (Cl) from September 2020 to August 2021 at an urban site located in Haizhu

117 wetland park of Guangzhou, which is surrounded by commercial streets and residential buildings,

118 however, with a distance of at least 1 km (Liu et al., 2022). Therefore, measurements at this site are

119 representative of the pollution characteristics of Guangzhou urban area. More detailed descriptions

120 about the sampling site and the ACSM measurements could be referred to Liu et al. (2022) and Ng et

121 al. (2011), respectively. An AE33 aethalometer (Drinovec et al., 2015) set up with a flow rate of 5

122   L/min was separately operated downstream of a $PM_{2.5}$ inlet (BGI SCC 1.829) to measure aerosol

123   absorptions, from which black carbon (BC) mass concentrations in winter and early spring. In addition,

124   mass concentrations of $PM_{2.5}$ and trace gases such as nitrogen dioxide (NO_2), ozone (O_3), carbon

125   monoxide (CO) and sulfur dioxide (SO_2) were acquired from the publicly available datasets of the

126   China National Environmental Monitoring network (http://www.cnemc.cn/en/), which includes a site

127   located within 5 km distance to our observation site. Measurements of meteorological parameters such

128   as temperature, wind speed and direction (WS and WD), and relative humidity (RH) were made by an

129   automatic weather station (Li et al., 2021). Aerosol liquid water content (ALWC) was predicted with

130   the ISORROPIA-II thermodynamic model in reverse mode under metastable assumption (Guo et al.,

131   2017) with aerosol chemical compositions measured by Q-ACSM as inputs, with more details in

132   Supplement Sect.S2.

133   **2.2 Q-ACSM data analysis**

134   The Q-ACSM data were processed using ACSM standard data analysis software (ACSM Local

135   1.5.10.0 Released July 6, 2015) written in Igor Pro (version 6.37). The composition-dependent

136   collection efficiency (CE) parameterization scheme proposed by Middlebrook et al. (2012) was chosen

137   to determine the mass concentrations of $NR-PM_1$ species which was also detailed in Liu et al. (2022).

138   Relative ionization efficiencies (RIEs) of 5.15 and 0.7 were adopted for ammonium and sulfate

139   quantifications which were calibrated using 300 nm pure NH_4NO_3 and $(NH_4)_2SO_4$ while the default

140   RIEs of 1.4, 1.1 and 1.3 was used for organic aerosol, nitrate and chloride, respectively. Moreover, we

141   also compared the mass concentrations of $NR-PM_1$ with $PM_{2.5}$ to ensure the validity of ACSM data

142   during the whole study. As shown in Fig. S1 of the supplement, the measured $NR-PM_1$ correlates

143   highly with $PM_{2.5}$ acquired from the nearest (about 5 km) Environmental Protection Agency site ($R^2 =$

144   0.71), and the average ratio of $NR-PM_1/PM_{2.5}$ is 0.77 (±0.36).

145   Unconstrained Positive matrix factorization (PMF) was performed on OA mass spectra of the entire

146   year-long dataset. For the two-factor solution, the POA factor peaked in the evening with low O/C

147   (~0.28) and an oxygenated OA (OOA) factor peaks in the afternoon with high O/C (~0.88) can be well

148   resolved (Fig.S2), demonstrating the markedly different influences of primary emissions and SOA

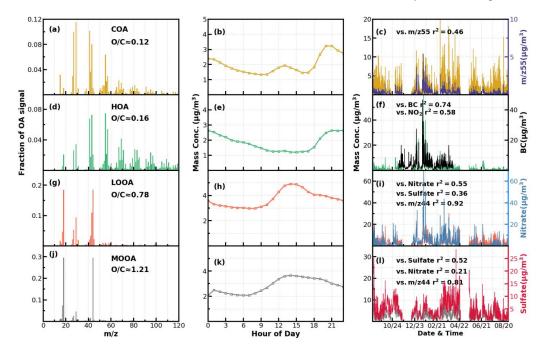149   formations on diel aerosol mass concentrations. However, PMF-ACSM analysis of mass spectra of

Figure 1. Mass spectral profiles, diurnal cycles and correlations with external data of COA**(a-c)**, HOA**(d-f)**, LOOA**(g-i)** and MOOA**(j-l)** from ME2-ACSM analysis for the entire year.

150   OA measured by unit mass resolution instruments still faced some uncertainties to further resolve

151   potential POA or SOA components due to its rotational indeterminacy. For example, traffic-related

152   hydron-carbon like organic aerosols (HOA) was uneasily to separate from cooking-related organic

153   aerosols (COA) and there was also great uncertainty in distinguishing SOA with different degrees of

154   oxidations (Sun et al., 2012;Sun et al., 2013;Zhang et al., 2015). Therefore, an improved source

155   apportionment technique called Multilinear Engine (ME-2) was further used to resolve better sources

156   of POA and SOA (Paatero, 1999;Canonaco et al., 2013;Guo et al., 2020). Previously, both Guo et al.

157   (2020) and Liu et al. (2022) demonstrated that during both autumn and winter seasons of Guangzhou

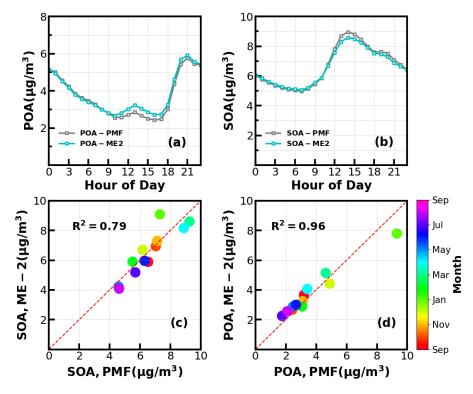158   urban areas, POA was mainly composed of HOA, which is mostly associated with traffic emissions

159 and COA, and SOA could be resolved into less oxidized and more oxidized organic aerosols (LOOA

160 and MOOA). The number selecting test using unconstrained PMF analysis (Fig.S3) also showed that

161 four-factor solution likely be the best choice. Therefore, we had chosen 4 factors for ME-2 analysis

162 with the a value of ME-2 ranges from 0.1 to 0.5, and constrained the HOA and COA profiles with

163 HOA and COA profiles reported in Liu et al. (2022) as priories considering the following three reasons:

164 (1) The used instrument of this study is the same one of Liu et al. (2022); (2) the COA profile reported

165 in Liu et al. (2022) was determined during the period when both COVID-19 silence-action and festival

166 spring occurred when cooking activities grew and traffic activities almost vanished thus COA shall

167 dominated over HOA, more details about the method please refer to Liu et al. (2022); (3) Resolved

168 variations of HOA and COA are well explained by external datasets such as correlations of HOA with

169 black carbon reached 0.79. The four-factor solution using the ME-2 technique with a=0.2 was obtained

170 and shown in Fig.1. The resolved HOA and COA are summed as POA, resolved LOOA and MOOA

171 are summed as SOA, and the comparison with those resolved by the PMF is shown in Fig.2. ME-2

172 analysis generally reproduced both the diurnal variations as well as absolute mass concentrations of

173 POA and SOA during different months well. To explore the consistency of resolved factors using the

174 entire year-long dataset or only using seasonal dataset when performing ME-2 analysis, we performed

175 individual ME-2 runs for each season. Results showed that factors resolved in each season using

176 seasonal datasets as inputs of ME-2 are generally consistent with those resolved from year-long dataset

177 (Fig.S4-S7). Therefore, factors resolved using the entire year-long dataset as input of ME-2 were used

178 for further investigations and this also guaranteed consistency of factors for comparisons among
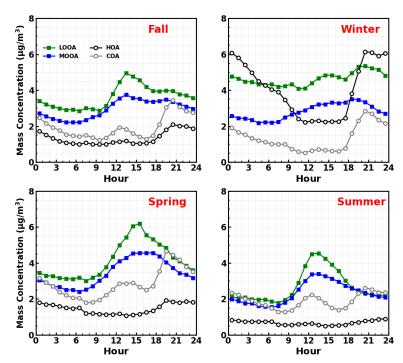
179 seasons.

Figure 2. (a) and **(b)** Diurnal variations of POA and SOA concentrations from ME-2 and PMF; **(c)** and **(d)** Scatter plots between monthly average POA and SOA concentrations from ME-2 and PMF.

180   The mass spectrum of COA deconvolved in this work was characterized by a high m/z 55-to-57

181   ratio of 2.12, which was the same with the one reported by Guo et al. (2020), and close to the m/z 55-

182   to-57 ratio range of 2.2-2.8 reported by Mohr et al. (2012) for COA. Similar to previous studies (Guo

183   et al., 2020;Sun et al., 2013), the concentration of COA was well correlated (R^2=0.46) with m/z 55.

184   The O/C ratio of 0.12 for COA revealed that it was less oxidized than HOA (O/C=0.16) during the

185   whole year in Guangzhou, which was contrary to Sun et al. (2011). As shown in Fig.3, the diurnal

186   profile of COA presented two typical peaks during the entire year with a noontime peak during 13:00

187   - 14:00 LT and an evening peak during 20:00 - 21:00 LT, which were associated with noon and evening

188   cooking activities. It was noteworthy that the nighttime peak concentration of COA was very close to

189   that of noontime in summer, while the evening peak of COA was significantly higher than that of

190   noontime in other three seasons. The ratio of evening COA peak to that of the noontime was 1.7 in fall,

191   and was 1.6 in spring. In particular, the evening COA peak was nearly 4 times that of noontime in

192   winter due to the relatively insignificant noontime peak during this period, which might be associated

193 with the lock down and spring festival in winter which resulted in less noontime activities. Similar

194 conclusions could be found in Sun et al. (2018). More frequent cooking activities at night such as the

195 Chinese habit of eating midnight snacks, shallower boundary layer that inhibited diffusion of pollutants,

196 and the lower temperature at night which facilitated semi-volatile compounds from cooking emissions

197 to partition into particles resulted in the higher peak concentration at nighttime than at noon (Guo et

198 al., 2020).

Figure 3. Diurnal profiles of HOA, COA, LOOA and MOOA in spring (March to May), summer (Jnue to August), Fall (September to November), Winter (December to February).

199 The mass spectrum of HOA (Fig.1b) was characterized with the $C_nH_{2n-1}^+$ (m/z = 27, 41, 55, 69)

200 and $C_nH_{2n+1}^+$ (m/z = 29, 43, 57, 71) ion species. The concentration of HOA had a good correlation

201 with that of primary BC emission (R^2=0.74), and also correlated well with that of NO_2 (R^2=0.58),

202 indicating considerable impacts of traffic emissions on the HOA mass loading. As shown in Fig.3,

203 except for summer, HOA increased significantly after sunrise especially in winter, however, began to

204 decrease in the late evening. HOA was significantly higher during nighttime than during daytime in

205 all seasons especially in winter, however, was not obvious in summer. HOA mass concentration peaks

206 around 20:00 LT were attributed to traffic emissions during the nocturnal rush hours. However, the

207 continuously high concentrations of HOA after 20:00 until 02:00 of the next day might have resulted

208 from heavy-duty vehicles with daytime traffic restrictions in Guangzhou (Guo et al., 2020;Qin et al.,

209 2017).

210 Two OOA factors were characterized with high O/C ratio, LOOA with O/C of 0.78 and MOOA

211 with O/C of 1.2, suggesting high oxidation degrees of SOA factors in Guangzhou urban area, especially

212 that of MOOA. MOOA and LOOA shared similar diurnal profiles regardless of seasons, with MOOA

213 showed higher correlations with sulfate and LOOA showed higher correlations with nitrate. MOOA

214 and LOOA increased together in fall from 09:00 LT until 14:00 LT reached a maximum of 3.7 $\mu g/m^3$

215 for MOOA and 5 $\mu g/m^3$ for LOOA, followed by a gradual decrease in SOA concentrations and then

216 remained relatively flat. The diurnal profiles of SOA in spring and summer were relatively similar to

217 those in fall, however, more remarkable decreases of SOA from afternoon to midnight were observed

218 in spring and summer. This is because SOA sometimes increased after sunset in autumn, which was

219 even more prominent in winter, where LOOA and MOOA would first increase for a while after sunset

220 and then begun to decrease. However, weaker daytime SOA formation was observed in winter.
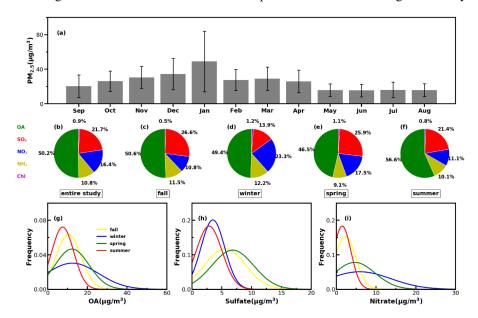
221 **3 Results and discussion**

222 **3.1 The largest contribution of secondary organic aerosols in NR-PM$_1$**

223 Time series of the meteorological parameters (including RH, WS and WD), the mass

224 concentrations of NR-PM$_1$ and PM$_{2.5}$, chemical compositions of NR-PM$_1$, trace gases and four

225 resolved OA factors are shown Fig.S8. It shows that emission source intensities and meteorological

226 variables changed dramatically among seasons. Hourly NR-PM$_1$ mass concentrations ranged from near

227 zero to 177 $\mu g/m^3$ with an average of 21 $\mu g/m^3$. From October to February, northerly winds prevailed

228 and average NR-PM$_1$ was relatively higher than that from February to September (26 vs 19 $\mu g/m^3$),

229 which were associated with relatively lower boundary height during cold seasons and northern winds

230 brought polluted continental air mass. While during warm seasons of Guangzhou (March to

231 September), south-easterly wind prevailed, which brought cleaner air mass from the ocean and the

232 boundary layer height was higher due to more surface heating. Monthly variations of PM$_{2.5}$ are shown

233 in Fig.3a, PM$_{2.5}$ in summer was lowest and around 16 $\mu g/m^3$ from May to August which were likely

234 associated with the prevalence of rainy conditions in summer and possible higher boundary layer

235 height. January was the month with highest $PM_{2.5}$ mass concentrations with an average of 49 μg/m^3,

236 which was consistent with the fact that winter usually experienced the worst air pollutions due to the

237 stagnant air conditions.

238 The average mass contributions of different components to $NR\text{-}PM_1$ during the entire year and

Figure 3. (a) Monthly average $PM_{2.5}$ mass concentrations from September of 2020 to August of 2021; **(b)-(f)** The average mass fractions of the chemical components in $NR\text{-}PM_1$ of the entire year and different seasons; **(g)-(i)** Probability distributions of OA, sulfate (SO_4) and nitrate (NO_3) in different seasons.

239 among different seasons are shown in Fig.3b-3f. On average OA contributed about 50% to $NR\text{-}PM_1$

240 with the highest contribution in summer that reached near 57% and lowest contribution in spring of

241 about 47%. The second largest contributor was sulfate, which on average contributed about 22%, and

242 more than 20% in spring, summer and fall. However, the contribution of nitrate to $NR\text{-}PM_1$ (23%)

243 exceeded that of sulfate (14%) and became the second major component after OA in winter, consistent

244 with the results of Guo et al. (2020) for pollution periods in winter of Guangzhou. The probability

245 distributions of mass concentrations of OA, sulfate and nitrate are shown in Fig.3g-3i. Both OA and

246 nitrate were distributed in wide ranges during winter and shared similar shape of probability

247 distribution, with OA increasing gradually from summer to winter and then reducing in the spring.

248 Sulfate shared similar magnitudes in summer and winter, and differed much from those in spring and

249   fall that had higher sulfate concentrations and varied in a wider range. Nitrate in summer and fall were

250   relatively lower in summer and fall, however, had much higher concentrations in spring and winter.

251   As shown in Fig.4a, average OA concentrations of different months ranged from about 7 μg/m^3

252   to 17 μg/m^3 with the peak in January and the lowest in August, and the variations of OA mass

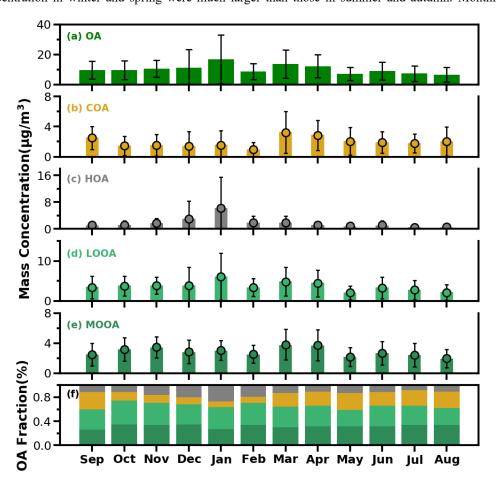253   concentration in winter and spring were much larger than those in summer and autumn. Monthly

Figure 4. The bar plots of monthly average mass concentrations of OA, COA, HOA, LOOA and MOOA from (a) to (e) and mass fractions of OA factors in OA (f).

254   variations of mass concentrations of the four resolved factors are shown in Fig.4b-e, and contributions

255   of the four OA factors to OA are shown in Fig.4f. In general, HOA remained lower than 2 μg/m^3 in

256   most months, however, as the cold season approached from November, the monthly average OA

257   increased substantially from about 2 μg/m^3 to near 6 μg/m^3. The much lower temperature and

258   accumulation favorable meteorological conditions likely had resulted in the substantial increase of

259   HOA. The obviously higher concentrations of NO_2 even under lower wintertime O_3 concentrations

260   (Fig.S8) implied that more traffic emissions in winter might also had contributed to the substantial

261   HOA increase. Compared with HOA, the seasonal variations of COA were less pronounced. The

262   monthly average concentration of COA in warm months (February to October) was higher than those

263   in cold months (October to January). The lowest monthly average concentration of COA was about

264   1 $\mu g/m^3$ which occurred in February when the contribution of COA to OA was near its lowest of about

265   9%. Overall, the contributions of COA to OA were higher than that of HOA during warm months,

266   however, lower than that of HOA in relatively cold months especially in winter, and contributed about

267   19% of OA during the whole year, which was close to that of HOA (18%). These results highlight the

268   significant contributions of POA to OA in Guangzhou urban area, however, contributions of emission

269   sources differed much among cold and warm seasons.

270   SOA (MOOA+LOOA) contributed more than 60% to OA in all months, reached beyond 70% in

271   October and February, and made up on average 63% of OA in the entire year. As shown in Fig.4(e-f),

272   LOOA exhibited stronger seasonal variations than MOOA, with monthly average mass concentrations

273   of LOOA varying between 2.6 to 6.1 $\mu g/m^3$ and monthly average MOOA concentration ranging from

274   2 to 3.8 $\mu g/m^3$. The LOOA mass concentration peaked in the most polluted month of January,

275   suggesting that significant contributions of LOOA formation to severe haze pollution in winter. The

276   contribution of LOOA to OA ranged from 27% to 39% with an average of 34%, and the contribution

277   of MOOA to OA ranged from 26% to 35% with an average of 32%. Overall, the average mass

278   concentration of SOA was about 1.7 times that of POA for the whole year, and SOA accounted for

279   about 32% of NR-PM$_1$, which was higher than those of sulfate and nitrate, demonstrating the largest

280   contribution of SOA to NR-PM$_1$.

281   **3.2 Significant contributions of secondary organic aerosols to haze formations in all seasons**

282   Investigations on contribution variations of aerosol compositions under different aerosol pollution

283   levels are helpful for understanding mechanisms of haze formations, and results in four seasons are

284   presented in Fig.5. The chemical composition of NR-PM$_1$ under different pollution levels differ much

285   among seasons. In fall, as demonstrated by variations of mass concentrations of aerosol compositions
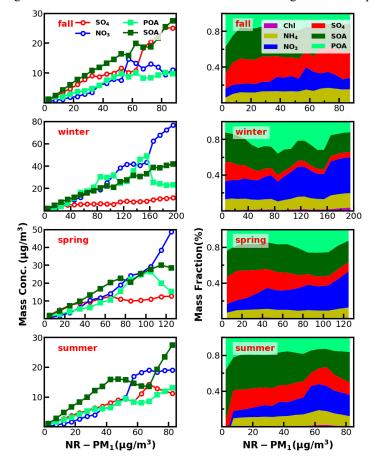
286   under different pollution levels shown in Fig.5, pollution conditions in fall were dominantly controlled

287   by secondary formations of sulfate and SOA, accumulation of primary aerosols and nitrate formation

288   had relatively smaller impacts. With respect to mass fractions variations, contributions of aerosol

289   components differed much among different pollution levels. The fraction of OA decreased rapidly from

290   67% to 50% when the mass concentration of NR-PM$_1$ gradually increased to 15 μg/m^3, while the

291   contribution of sulfate increased substantially from 17% to 30%, and the contribution of nitrate

292   remained relatively stable at about 10%. When NR-PM$_1$ further increased, OA contribution remained

293   relatively flat for NR-PM$_1$ below about 50 μg/m^3. Accordingly, the contribution of SO$_4^{2-}$ decreased to

294   ~18%, and the contribution of nitrate substantially increased from ~10 % to 21%. After that, OA

295   contribution decreased rapidly to about 40% and then remained stable for NR-PM$_1$ >50 μg/m^3.

296   However, the contribution of sulfate began to increase, and the highest contribution could account for

297   30%, while the contribution of nitrate began to decline gradually to 12%. In addition, the SOA

298   contributed dominantly to OA (>60%) for NR-PM$_1$ > 15 μg/m^3 and even reached near 70% for NR-

299   PM$_1$ > 35 μg/m^3, suggesting the dominant role of SOA in OA accumulations in haze events during fall.

300   In winter, haze formations are mostly associated with POA accumulations, SOA and nitrate

301   formations, with nitrate formation playing the most important role, since it is also accompanied by

302   ammonium formation, while sulfate formation was weak in winter. The fraction of OA increased

303   gradually with the increase of NR-PM$_1$ concentration for NR-PM$_1$ < 90 μg/m^3 and reached the

304   maximum of 60%, while the contribution of nitrate also showed a small increase from 21% to 26%.

305   Under aggravating pollution, OA contribution fluctuated, however, showed a decreasing trend from

306   60% to ~40%. Meanwhile, the nitrate contribution showed an increasing trend from 26% to ~40%,

307   which was similar to that of OA. Sulfate contribution decreased with the increase of NR-PM$_1$

308   concentration for NR-PM$_1$ < 100 μg/m^3 and then remained at about 6% as NR-PM$_1$ increases. In

309   addition, the POA contribution increased about 25% to 50% for NR-PM$_1$ < 100 μg/m^3. Overall, the

310   increase of nitrate, POA and SOA together had resulted in severely polluted conditions in winter. The

311   substantial contribution of POA to severe haze demonstrates that meteorological conditions

312   unfavorable for the pollutant diffusion together with the substantial contributions of secondary nitrate

313   and SOA formations have resulted in the most severe haze pollutions among the year. Especially, HOA

314   contribution to OA increased from 17% to 52% when NR-PM$_1$ concentration was less than 140 μg/m^3,

315   suggesting the significant role of traffic emission accumulation during severe haze pollution, which

Figure 5. Left panels show absolute mass concentration variations of aerosol compositions under different NR-PM$_1$ levels, right panels show mass fractions of chemical components as a function of NR-PM$_1$.

316   was consistent with results of Yao et al. (2020).

317   In spring, haze pollutions were mostly associated POA accumulation and secondary formations of

318   nitrate and SOA, especially that of nitrate. The contribution of OA decreased from 51% to 44% as NR-

319   PM$_1$ mass concentration increased when NR-PM$_1$ mass concentration was less than 50 μg/m^3. When

320   the mass concentration of NR-PM$_1$ reached about 105 μg/m^3, the fraction of OA reached a maximum

321   of 55%, and then decreased to about 37%. The most noticeable characteristic was the increase of nitrate

322   contribution (from 10% to 40%) and decrease of sulfate contribution (32% to 10%) as the NR-PM$_1$

323   increased. In summer, secondary aerosol formations contributed dominantly to haze formations, with

324   POA contribution to NR-PM$_1$ was about 20% in most conditions. The overall contribution of OA

325   gradually decreased from near 60% to 35% as the mass concentration of NR-PM$_1$ increased for NR-

326   PM$_1$ concentration < 60 μg/m^3 which was markedly different with those in other seasons, however

327   increased to 49% as the NR-PM$_1$ concentration increased further. The contribution of sulfate decreased

328   from 25% to 13% and the contribution of nitrate increased from 9.0% to 31% with the increase of NR-

329   PM$_1$ concentration for NR-PM$_1$ concentration < 60 μg/m^3. While the OA was dominated by SOA under

330   most conditions (about 60%).

331   Overall, haze formation mechanisms differed much among distinct seasons. Sulfate mattered more

332   than nitrate in   fall, while nitrate mattered more than sulfate in spring and winter, however, SOA

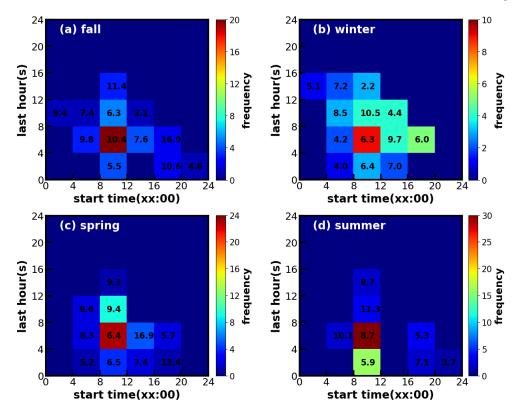333   contributed significantly to haze formations in all seasons.

334

3.3 Discussions on SOA formation mechanisms

336   SOA can be formed through condensation of oxidized gas-phase organic vapors during the

337   oxidation of volatile organic compounds (VOCs), this type of formed SOA was usually referred to as

338   gasSOA (Kuang et al., 2020). SOA can also be formed in the aqueous phase through the further

339   oxidation of dissolved VOCs which are usually products of gas-phase oxidation of VOCs, this type of

340   SOA was usually referred as aqSOA (Kuang et al., 2020). As shown in Fig.3, both LOOA and MOOA

341   mainly increased after sunrise, highlighting important roles of photochemistry in SOA formations.

342   However, as demonstrated by Kuang et al. (2020), the daytime SOA formation could be either result

343   from gas-phase photochemistry and subsequent condensation (gasSOA), or the result of gas-phase

344   VOCs transformations with subsequent aqueous reactions (aqSOA). Especially since the PRD region

345   is characterized by both active photochemistry due to strong solar radiation in subtropical regions and

346   high relative humidity (annual average RH of ~75%), both photochemistry and aqueous phase

347   reactions might play significant roles in SOA formation, however, this aspect was not explored before.

348   Considering the frequent co-increase of MOOA and LOOA, they were grouped together as SOA

349   for further investigations on their formation. SOA formation cases in four seasons were identified, the

350   start time and lasting hours of their occurrences, as well as associated SOA levels are shown in Fig.6.

351   Note that the identification of SOA formation cases has not considered the dilution effect of the lifting

Figure 6: Time frequency diagrams of SOA increase events in **(a)** fall, **(b)** winter, **(c)** spring and **(d)** summer. X-axis represent start time of SOA increase, and y-axis represents the lasting hours of SOA increase events. The color scales indicate the number of occurrences. The values in the grid are the average SOA concentration during the SOA increase case.

352   daytime boundary layer height and was only based on the absolute mass concentration variations.

353   Therefore, this method has neglected some SOA formation cases that were masked by evolutions of

354   the boundary layer, and the identified cases represent active SOA formation events that overcame

355   dilution effects, which might be more suitable for further SOA formation investigations due to strong

356   SOA formation signals. It shows that in all seasons, the SOA formation happened most frequently

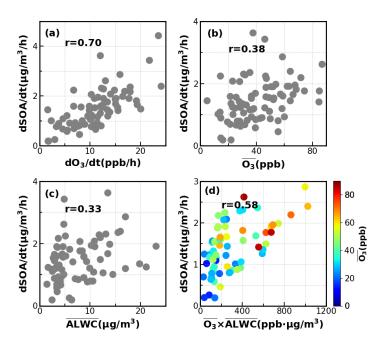357   during daytime, starting in the morning and lasting about 4-8 hours. Especially, in spring, summer and

358 fall, the daytime SOA formation almost happened everyday (Fig.S5-7), even if strong daytime

359 boundary layer evolutions could be expected in these seasons due to strong surface solar heating, and

360 resulted in the afternoon SOA mass concentration peaks in these seasons (Fig.3). However, highest

361 SOA concentrations did not appear in the seasons with the most frequent morning to afternoon

362 increases. Taking SOA formation cases in spring as an example, if the SOA increase started in the

363 morning, more than 8 hours duration will result in significant higher SOA concentration. These cases

364 started in the afternoon and lasted 4-8 hours would result in highest SOA concentration in spring. The

365 SOA formation cases starting in the morning, however, only lasting within 4 hours, happened

366 frequently in summer while less in spring and fall, suggesting that the absolute SOA mass

367 concentration increase was more often stopped by strong boundary layer mixing in summer, which

368 was consistent with the solar heating characteristics. The highest SOA in fall and winter were

369 associated with the continuous increase of SOA after sunrise, suggesting that coordination of daytime

370 and nighttime SOA formation together had resulted in the highest SOA concentrations in fall and winter.

371   To dig deeper into possible mechanisms behind the active daytime SOA formations throughout

372 the year, we investigated relationships between SOA formation rates and both O_3 as well as aerosol

373 liquid water content (ALWC) for the most frequent morning to afternoon SOA increase cases. Without

374 considering the dilution effect of rising boundary layer, the daytime apparent growth rates of SOA

375 varied from 0.2 to 4.4 μg m^{-3} h^{-1} (Fig.7). Note that the SOA growth rates was calculated on the basis

376 of observations of the first four hours for each SOA increase case to reduce impacts of boundary layer

377 dilution effects. Some previous studies used variations of CO concentrations to partially correct for

378 boundary layer dilution effects, however this method would fail in sites with strong CO emissions

379 (Kuang et al., 2020). The SOA growth rates and were highly correlated to O_3 formation rates (r=0.7)

380 as shown in Fig.7. However, this result only proved the important role of photochemistry in SOA

381 formations. The apparent SOA growth rates showed positive but much weaker correlation with the

382 average O_3 concentration during the period of SOA the increase (r=0.38), demonstrating that oxidant

383 level was likely not the controlling factor for SOA formation, although O_3 alone did not represent the
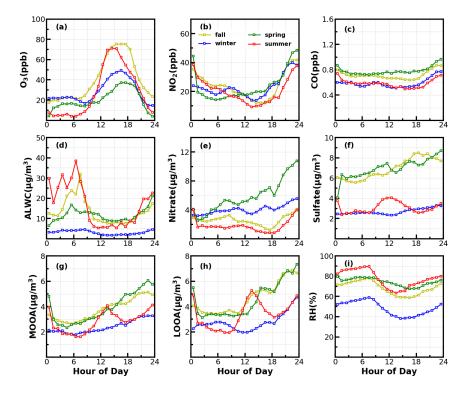
Figure 7. Relationships between SOA daytime formation rates with corresponding **(a)** O_3 formation rate; **(b)** average O_3; **(c)** average ALWC ($\mu g/m^3$) and **(d)** combination of averaged O_3 and averaged ALWC.

variations of oxidation levels and other sources such as HONO photolysis (Yu et al., 2022) also contribute to OH radicals and is a typical oxidant in daytime photochemistry. To investigate the possible roles of aqueous reactions in SOA formation, the relationship between apparent SOA rates and corresponding average ALWC were also investigated, and a positive but weak correlation was found (r=0.33). More importantly, the correlation coefficient between apparent SOA growth rates and the variable of average ALWC multiplying by average O_3 would be much higher (r=0.58, Fig.7d), suggesting that the coordination of gas-phase photochemistry and further aqueous reactions had likely resulted in the rapid daytime SOA formations.

392   Besides the daytime SOA formation associated with photochemistry, dark transformations of

393   VOCs that involve nighttime gas-phase and aqueous phase reactions might also result in efficient SOA

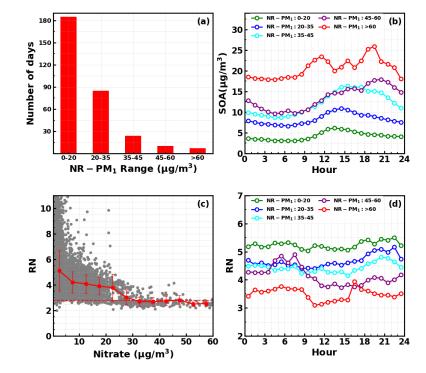394   formations. As shown in Fig.6, continuous increases of SOA were also frequently observed after sunset

Figure 8. Average diurnal variations of **(a)** O_3; **(b)** NO_2; **(c)** CO; **(d)** ALWC; **(e)** nitrate; **(f)** sulfate; **(g)** MOOA; **(h)** LOOA and **(i)** RH for identified days with nighttime SOA increases.

395   in spring (17 days), fall (18 days) and winter (20 days) with sporadic occurrence in summer, and the

396   coordination of daytime and nighttime SOA formations together have resulted in the highest SOA

397   concentrations in fall and winter which were associated with severe haze pollutions as demonstrated

398   above. Average diurnal profiles of O_3, NO_2, CO, RH, ALWC, nitrate, sulfate, LOOA and MOOA for

399   cases with co-increases of LOOA and MOOA after 18:00 in different seasons are shown in Fig.8. On

400   average, SOA usually showed decreases during nighttime (Fig.3) due to transport of air mass from

401   cleaner suburban regions. The average wind speed was 1.7 m/s from 18:00 to 23:00 LT for identified

402   nighttime SOA increase cases and was obviously lower than the corresponding average wind speed of

403   2.3 m/s, suggesting the more stagnant air mass tended to favor the nighttime SOA increases. However,

Atmospheric
Chemistry
and Physics
Discussions

404 the nighttime 5h back trajectories shown in Fig.S9 demonstrated that the nighttime replacement of

Figure 9. **(a)** Number of days in different daily average NR_PM$_1$ ranges; **(b)** Diurnal profiles of SOA under different NR_PM$_1$ ranges; **(c)** Variations NO+/NO2+ (RN) as a function of measured nitrate, horizontal dashed line corresponds to RN of 2.8, red markers and bars represents averages and standard deviations; **(d)** Diurnal profiles of RN under different NR_PM$_1$ ranges.

405 surrounding suburban cleaner air mass still prevailed, therefore the continuous increases of SOA

406 suggested that nighttime SOA formation occurred on a regional scale. The increases of LOOA and

407 MOOA were accompanied with obvious nitrate formation in all seasons as well as slight increases of

408 sulfate, further indicating for regional scale nighttime secondary aerosol formations during these

409 nighttime SOA formation events. Except for summer, continuous increase of SOA from the morning

410 to nighttime confirmed that the coordination of daytime and nighttime SOA formations had contributed

411 to haze formations. Number of days for daily average NR-PM$_1$ ranges of 0-20, 20-35, 35-45, 45-60

412 and >60 μg/m^3 were 185,85,24,10 and 7, respectively (Fig.9a). All cases with daily average NR-PM$_1$

413 higher than 45 μg/m^3 occurred in fall, winter and spring. The corresponding average diurnal variations

414 of SOA for these relatively severe conditions shown in Fig.9b confirmed further that the coordination

415   of daytime and nighttime SOA formations had contributed to severe haze formations in Guangzhou

416   urban area.

417   The NO_3 radical formed through the rection between NO_2 and O_3 is the typical nighttime oxidant.

418   Results of Rollins et al. (2012) and Kiendler-Scharr et al. (2016) revealed that NO_3 oxidation of VOCs

419   would contribute substantially to nighttime SOA increase. As shown in Fig.8a, after sunset, the O_3

420   concentration decreased quickly, however, remained substantially higher than zero, accompanied was

421   the remarkable increases of NO_2 and nitrate. In Guangzhou urban areas, nitrate can either be formed

422   through gas-phase oxidation of NO_2 by OH which forms HNO_3 and then condenses onto aerosol phase,

423   or be formed through the hydrolysis of N_2O_5, which is formed through reactions between NO_2 and

424   NO_3 radical (Yang et al., 2022). The obvious co-increases in nitrate and SOA after sunset indicated

425   that the decrease of O_3 and increase of NO_2 consumption had supplied the NO_3 and N_2O_5 reaction

426   chains and the increase of ALWC favored the hydrolysis of N_2O_5. This was indirectly confirmed when

427   during winter, despite relatively high concentrations of O_3 and NO_2 after sunrise compared with other

428   seasons, nitrate formation was much less prominent due to substantially lower ALWC associated with

429   lower RH. However, the quick increase of SOA still occurred after sunset despite weak daytime SOA

430   formation, suggesting that aqueous reactions might play minor roles in nighttime SOA formation that

431   involve NO_3 radical in Guangzhou urban area. The nighttime chemistry that involves NO_3 radical

432   might contribute substantially to organic nitrate formation (Ng et al., 2008;Fry et al., 2009;Rollins et

433   al., 2012) which would produce the same ions (NO+ and NO2+) with inorganic nitrate due to the

434   fragmentation of nitrate functionality (-ONO2) under 70 eV electron ionization in the aerosol mass

435   spectrometer measurements. However, organic nitrate has different fragmentation pattern with that of

436   inorganic nitrate with previous laboratory studies have shown that the RN=NO+/NO2+ of organic

437   nitrate is substantially higher than that of inorganic nitrate. Farmer et al. (2010) thus proposed that the

438   RN variations can be used as an indicator of organic nitrate formations. The Q-ACSM measurements

439   with unit mass resolution cannot provide accurate measurements of RN due to the resolution limitation

440   (Allan et al., 2004), however, the resolved RN related to measured nitrate might provide qualitative

441   constraints on impacts of organic nitrates. The variations of resolved RN as a function of measured

442   nitrate are shown in Fig.9c, which shows that at high levels of nitrate when inorganic nitrate usually

443   dominates (Xu et al., 2021), the RN approaches near 2.8 which was close to the inorganic nitrate RN

Atmospheric
Chemistry
and Physics
Discussions

Open Access

EGU

444   reported in (Xu et al., 2021), and locates in the range of 1.1-3.5 of inorganic nitrate RN reported in

445   literatures (Xu et al., 2015b). Diurnal variations of RN under different pollution levels shown in Fig.9d

446   reveals higher nighttime RN than daytime, and obvious continuous increase of RN after sunset can be

447   observed for relatively clean and polluted conditions (daily average NR-PM$_1$ of 20-35 μg/m^3 to NR-

448   PM$_1$ of 45-60 μg/m^3), suggesting active nighttime organic nitrate formations, which confirmed the

449   involvement of NO$_3$ radicals in nighttime SOA formations.

450   **4 Implications for future studies**

451   In this study, we highlighted the significant roles of SOA in haze formations in Guangzhou urban

452   area during the entire year and pointed out that for the most prominent and frequent daytime SOA

453   formations all the year around, both gas-phase photochemistry and aqueous reactions played

454   significant roles. Therefore, daytime SOA formation was weak in winter when oxidant level and RH

455   were low, whereas prominent SOA formations were be observed in fall, spring and summer on almost

456   daily basis. However, how gas-phase and aqueous phase reactions have coordinated to promote the

457   SOA formation, and the different contributions of gasSOA and aqSOA to SOA formations under

458   different meteorological conditions and VOCs profiles in different seasons are not clear. In addition,

459   our results suggested that the coordination of daytime and nighttime SOA formation together had

460   resulted in highest SOA concentrations in Guangzhou urban area, thus contributed significantly to

461   severe haze formation. The co-increases of nitrate and SOA after sunrise indicated the significant roles

462   of nighttime NO$_3$ radical chemistry in promoting haze formations. However, our understanding on

463   how nighttime chemistry evolved and contributed to secondary aerosols formations in different

464   seasons is still highly insufficient in this region. Therefore, the precursors and formation pathways of

465   daytime and nighttime SOA formations and how they coordinated to promote severe haze formations

466   need further comprehensive investigations to make targeted emission control strategies to continuously

467   improve air quality in the PRD region. Also, findings of this study have important implications on

468   future investigations of SOA formation mechanisms in urban areas of southern China that share similar

469   emission sources and meteorological conditions.

470

471   **Data availability**. All data needed are presented in time series of Figures and supplementary Figures,

Atmospheric
Chemistry
and Physics
Discussions

472   raw datasets of this study are available from the corresponding author Li Liu (liul@gd121.cn) upon

473   request.

474

475   **Competing interests**. The authors declare that they have no conflict of interest.

476

477   **Author Contributions**. YK and LL designed the aerosol experiments. YK conceived and led this

478   research. MMZ and YK wrote the manuscript. MMZ and LL conducted the long-term Q-ACSM

479   measurements. MMZ and YH performed the PMF analysis. HBX, CY, YZ and FL helped maintain and

480   calibrating the Q-ACSM. CL provided meteorological datasets, BL performed the AE33 measurements

481   and post data processing. XJD obtained funding for the continuous aerosol measurements. JCT and

482   WYX provided insights into data analysis, and all authors contributed to revisions of this paper.

483

484

485   ## Acknowledgments

493

494   ## References

495   Allan, J. D., Delia, A. E., Coe, H., Bower, K. N., Alfarra, M. R., Jimenez, J. L., Middlebrook, A. M., Drewnick, F., Onasch,

496   T. B., Canagaratna, M. R., Jayne, J. T., and Worsnop, D. R.: A generalised method for the extraction of chemically

497   resolved mass spectra from Aerodyne aerosol mass spectrometer data, Journal of Aerosol Science, 35, 909‑922,

498   https://doi.org/10.1016/j.jaerosci.2004.02.007, 2004.

499   Allan, J. D., Williams, P. I., Morgan, W. T., Martin, C. L., Flynn, M. J., Lee, J., Nemitz, E., Phillips, G. J., Gallagher, M. W.,

500 and Coe, H.: Contributions from transport, solid fuel burning and cooking to primary organic aerosols in two UK

501 cities, Atmospheric Chemistry and Physics, 10, 647-668, 10.5194/acp-10-647-2010, 2010.

502 Canagaratna, M. R., Jayne, J. T., Jimenez, J. L., Allan, J. D., Alfarra, M. R., Zhang, Q., Onasch, T. B., Drewnick, F., Coe,

503 H., Middlebrook, A., Delia, A., Williams, L. R., Trimborn, A. M., Northway, M. J., DeCarlo, P. F., Kolb, C. E., Davidovits,

504 P., and Worsnop, D. R.: Chemical and microphysical characterization of ambient aerosols with the aerodyne aerosol

505 mass spectrometer, Mass Spectrom Rev, 26, 185-222, 10.1002/mas.20115, 2007.

506 Canonaco, F., Crippa, M., Slowik, J. G., Baltensperger, U., and Prevot, A. S. H.: SoFi, an IGOR-based interface for the

507 efficient use of the generalized multilinear engine (ME-2) for the source apportionment: ME-2 application to

508 aerosol mass spectrometer data, Atmos. Meas. Tech., 6, 3649-3661, 10.5194/amt-6-3649-2013, 2013.

509 Canonaco, F., Tobler, A., Chen, G., Sosedova, Y., Slowik, J. G., Bozzetti, C., Daellenbach, K. R., El Haddad, I., Crippa,

510 M., Huang, R. J., Furger, M., Baltensperger, U., and Prevot, A. S. H.: A new method for long-term source

511 apportionment with time-dependent factor profiles and uncertainty assessment using SoFi Pro: application to 1

512 year of organic aerosol data, Atmos. Meas. Tech., 14, 923-943, 10.5194/amt-14-923-2021, 2021.

513 Chen, W., Ye, Y. Q., Hu, W. W., Zhou, H. S., Pan, T. L., Wang, Y. K., Song, W., Song, Q. C., Ye, C. S., Wang, C. M.,

514 Wang, B. L., Huang, S., Yuan, B., Zhu, M., Lian, X. F., Zhang, G. H., Bi, X. H., Jiang, F., Liu, J. W., Canonaco, F., Prevot,

515 A. S. H., Shao, M., and Wang, X. M.: Real-Time Characterization of Aerosol Compositions, Sources, and Aging

516 Processes in Guangzhou During PRIDE-GBA 2018 Campaign, J Geophys Res-Atmos, 126, ARTN e2021JDO35114

517 10.1029/2021JD035114, 2021.

518 Drinovec, L., Močnik, G., Zotter, P., Prévôt, A. S. H., Ruckstuhl, C., Coz, E., Rupakheti, M., Sciare, J., Müller, T.,

519 Wiedensohler, A., and Hansen, A. D. A.: The "dual-spot" Aethalometer: an improved measurement of aerosol black

520 carbon with real-time loading compensation, Atmospheric Measurement Techniques, 8, 1965-1979, 10.5194/amt-

521 8-1965-2015, 2015.

522 Farmer, D. K., Matsunaga, A., Docherty, K. S., Surratt, J. D., Seinfeld, J. H., Ziemann, P. J., and Jimenez, J. L.: Response

523 of an aerosol mass spectrometer to organonitrates and organosulfates and implications for atmospheric chemistry,

524 Proceedings of the National Academy of Sciences, 107, 6670-6675, doi:10.1073/pnas.0912340107, 2010.

525 Fröhlich, R., Cubison, M. J., Slowik, J. G., Bukowiecki, N., Prévôt, A. S. H., Baltensperger, U., Schneider, J., Kimmel, J.

526 R., Gonin, M., Rohner, U., Worsnop, D. R., and Jayne, J. T.: The ToF-ACSM: a portable aerosol chemical speciation

527 monitor with TOFMS detection, Atmos. Meas. Tech., 6, 3225-3241, 10.5194/amt-6-3225-2013, 2013.

528 Fry, J. L., Kiendler-Scharr, A., Rollins, A. W., Wooldridge, P. J., Brown, S. S., Fuchs, H., Dubé, W., Mensah, A., dal Maso,

529 M., Tillmann, R., Dorn, H. P., Brauers, T., and Cohen, R. C.: Organic nitrate and secondary organic aerosol yield from

530 NO_3 oxidation of β-pinene evaluated using a gas-phase kinetics/aerosol partitioning model, Atmos.

531 Chem. Phys., 9, 1431-1449, 10.5194/acp-9-1431-2009, 2009.

532 Guo, H., Liu, J., Froyd, K. D., Roberts, J. M., Veres, P. R., Hayes, P. L., Jimenez, J. L., Nenes, A., and Weber, R. J.: Fine

533 particle pH and gas–particle phase partitioning of inorganic species in Pasadena, California, during the 2010 CalNex

534 campaign, Atmospheric Chemistry and Physics, 17, 5703-5719, 10.5194/acp-17-5703-2017, 2017.

535 Guo, J. C., Zhou, S. Z., Cai, M. F., Zhao, J., Song, W., Zhao, W. X., Hu, W. W., Sun, Y. L., He, Y., Yang, C. Q., Xu, X. Z.,

536 Zhang, Z. S., Cheng, P., Fan, Q., Hang, J., Fan, S. J., Wang, X. M., and Wang, X. M.: Characterization of submicron

537 particles by time-of-flight aerosol chemical speciation monitor (ToF-ACSM) during wintertime: aerosol

538 composition, sources, and chemical processes in Guangzhou, China, Atmospheric Chemistry and Physics, 20, 7595-

539 7615, 10.5194/acp-20-7595-2020, 2020.

540 He, L. Y., Huang, X. F., Xue, L., Hu, M., Lin, Y., Zheng, J., Zhang, R. Y., and Zhang, Y. H.: Submicron aerosol analysis

541 and organic source apportionment in an urban atmosphere in Pearl River Delta of China using high-resolution

542 aerosol mass spectrometry, J Geophys Res-Atmos, 116, Artn D12304

543 10.1029/2010jd014566, 2011.

544 Hu, W. W., Hu, M., Hu, W., Jimenez, J. L., Yuan, B., Chen, W. T., Wang, M., Wu, Y. S., Chen, C., Wang, Z. B., Peng, J.
545 F., Zeng, L. M., and Shao, M.: Chemical composition, sources, and aging process of submicron aerosols in Beijing:
546 Contrast between summer and winter, J Geophys Res-Atmos, 121, 1955-1977, 10.1002/2015jd024020, 2016.
547 Huang, R. J., Zhang, Y., Bozzetti, C., Ho, K. F., Cao, J. J., Han, Y., Daellenbach, K. R., Slowik, J. G., Platt, S. M., Canonaco,
548 F., Zotter, P., Wolf, R., Pieber, S. M., Bruns, E. A., Crippa, M., Ciarelli, G., Piazzalunga, A., Schwikowski, M., Abbaszade,
549 G., Schnelle-Kreis, J., Zimmermann, R., An, Z., Szidat, S., Baltensperger, U., El Haddad, I., and Prevot, A. S.: High
550 secondary aerosol contribution to particulate pollution during haze events in China, Nature, 514, 218-222,
551 10.1038/nature13774, 2014.
552 Huang, X. F., He, L. Y., Hu, M., Canagaratna, M. R., Kroll, J. H., Ng, N. L., Zhang, Y. H., Lin, Y., Xue, L., Sun, T. L., Liu, X.
553 G., Shao, M., Jayne, J. T., and Worsnop, D. R.: Characterization of submicron aerosols at a rural site in Pearl River
554 Delta of China using an Aerodyne High-Resolution Aerosol Mass Spectrometer, Atmospheric Chemistry and Physics,
555 11, 1865-1877, 10.5194/acp-11-1865-2011, 2011.
556 Jayne, J. T., Leard, D. C., Zhang, X. F., Davidovits, P., Smith, K. A., Kolb, C. E., and Worsnop, D. R.: Development of an
557 aerosol mass spectrometer for size and composition analysis of submicron particles, Aerosol Science and
558 Technology, 33, 49-70, Doi 10.1080/027868200410840, 2000.
559 Jimenez, J. L., Jayne, J. T., Shi, Q., Kolb, C. E., Worsnop, D. R., Yourshaw, I., Seinfeld, J. H., Flagan, R. C., Zhang, X. F.,
560 Smith, K. A., Morris, J. W., and Davidovits, P.: Ambient aerosol sampling using the Aerodyne Aerosol Mass
561 Spectrometer, J Geophys Res-Atmos, 108, Artn 8425
562 10.1029/2001jd001213, 2003.
563 Jimenez, J. L., Canagaratna, M. R., Donahue, N. M., Prevot, A. S. H., Zhang, Q., Kroll, J. H., DeCarlo, P. F., Allan, J. D.,
564 Coe, H., Ng, N. L., Aiken, A. C., Docherty, K. S., Ulbrich, I. M., Grieshop, A. P., Robinson, A. L., Duplissy, J., Smith, J. D.,
565 Wilson, K. R., Lanz, V. A., Hueglin, C., Sun, Y. L., Tian, J., Laaksonen, A., Raatikainen, T., Rautiainen, J., Vaattovaara, P.,
566 Ehn, M., Kulmala, M., Tomlinson, J. M., Collins, D. R., Cubison, M. J., Dunlea, J., Huffman, J. A., Onasch, T. B., Alfarra,
567 M. R., Williams, P. I., Bower, K., Kondo, Y., Schneider, J., Drewnick, F., Borrmann, S., Weimer, S., Demerjian, K., Salcedo,
568 D., Cottrell, L., Griffin, R., Takami, A., Miyoshi, T., Hatakeyama, S., Shimono, A., Sun, J. Y., Zhang, Y. M., Dzepina, K.,
569 Kimmel, J. R., Sueper, D., Jayne, J. T., Herndon, S. C., Trimborn, A. M., Williams, L. R., Wood, E. C., Middlebrook, A.
570 M., Kolb, C. E., Baltensperger, U., and Worsnop, D. R.: Evolution of Organic Aerosols in the Atmosphere, Science,
571 326, 1525-1529, 10.1126/science.1180353, 2009.
572 Kiendler-Scharr, A., Mensah, A. A., Friese, E., Topping, D., Nemitz, E., Prevot, A. S. H., Äijälä, M., Allan, J., Canonaco,
573 F., Canagaratna, M., Carbone, S., Crippa, M., Dall Osto, M., Day, D. A., De Carlo, P., Di Marco, C. F., Elbern, H., Eriksson,
574 A., Freney, E., Hao, L., Herrmann, H., Hildebrandt, L., Hillamo, R., Jimenez, J. L., Laaksonen, A., McFiggans, G., Mohr,
575 C., O'Dowd, C., Otjes, R., Ovadnevaite, J., Pandis, S. N., Poulain, L., Schlag, P., Sellegri, K., Swietlicki, E., Tiitta, P.,
576 Vermeulen, A., Wahner, A., Worsnop, D., and Wu, H.-C.: Ubiquity of organic nitrates from nighttime chemistry in
577 the European submicron aerosol, Geophysical Research Letters, 43, 7735-7744, 10.1002/2016gl069239, 2016.
578 Kuang, Y., He, Y., Xu, W., Yuan, B., Zhang, G., Ma, Z., Wu, C., Wang, C., Wang, S., Zhang, S., Tao, J., Ma, N., Su, H.,
579 Cheng, Y., Shao, M., and Sun, Y.: Photochemical Aqueous-Phase Reactions Induce Rapid Daytime Formation of
580 Oxygenated Organic Aerosol on the North China Plain, Environmental science & technology, 54, 3849-3860,
581 10.1021/acs.est.9b06836, 2020.
582 Li, Y. J., Lee, B. P., Su, L., Fung, J. C. H., and Chan, C. K.: Seasonal characteristics of fine particulate matter (PM) based
583 on high-resolution time-of-flight aerosol mass spectrometric (HR-ToF-AMS) measurements at the HKUST
584 Supersite in Hong Kong, Atmos. Chem. Phys., 15, 37-53, 10.5194/acp-15-37-2015, 2015.
585 Li, Z., Lei, L., Li, Y., Chen, C., Wang, Q., Zhou, W., Sun, J., Xie, C., and Sun, Y.: Aerosol characterization in a city in
586 central China plain and implications for emission control, J Environ Sci (China), 104, 242-252,
587 10.1016/j.jes.2020.11.015, 2021.

588 Liu, L., Kuang, Y., Zhai, M., Xue, B., He, Y., Tao, J., Luo, B., Xu, W., Tao, J., Yin, C., Li, F., Xu, H., Deng, T., Deng, X., Tan,
589 H., and Shao, M.: Strong light scattering of highly oxygenated organic aerosols impacts significantly on visibility
590 degradation, Atmos. Chem. Phys., 22, 7713-7726, 10.5194/acp-22-7713-2022, 2022.
591 Middlebrook, A. M., Bahreini, R., Jimenez, J. L., and Canagaratna, M. R.: Evaluation of Composition-Dependent
592 Collection Efficiencies for the Aerodyne Aerosol Mass Spectrometer using Field Data, Aerosol Science and
593 Technology, 46, 258-271, 10.1080/02786826.2011.620041, 2012.
594 Mohr, C., DeCarlo, P. F., Heringa, M. F., Chirico, R., Slowik, J. G., Richter, R., Reche, C., Alastuey, A., Querol, X., Seco,
595 R., Penuelas, J., Jimenez, J. L., Crippa, M., Zimmermann, R., Baltensperger, U., and Prevot, A. S. H.: Identification and
596 quantification of organic aerosol from cooking and other sources in Barcelona using aerosol mass spectrometer
597 data, Atmospheric Chemistry and Physics, 12, 1649-1665, 10.5194/acp-12-1649-2012, 2012.
598 Ng, N. L., Kwan, A. J., Surratt, J. D., Chan, A. W. H., Chhabra, P. S., Sorooshian, A., Pye, H. O. T., Crounse, J. D.,
599 Wennberg, P. O., Flagan, R. C., and Seinfeld, J. H.: Secondary organic aerosol (SOA) formation from reaction of
600 isoprene with nitrate radicals (NO$_3$), Atmos. Chem. Phys., 8, 4117-4140, 10.5194/acp-8-4117-2008,
601 2008.
602 Ng, N. L., Herndon, S. C., Trimborn, A., Canagaratna, M. R., Croteau, P. L., Onasch, T. B., Sueper, D., Worsnop, D. R.,
603 Zhang, Q., Sun, Y. L., and Jayne, J. T.: An Aerosol Chemical Speciation Monitor (ACSM) for Routine Monitoring of
604 the Composition and Mass Concentrations of Ambient Aerosol, Aerosol Science and Technology, 45, 780-794, Pii
605 934555189
606 10.1080/02786826.2011.560211, 2011.
607 Paatero, P.: The Multilinear Engine—A Table-Driven, Least Squares Program for Solving Multilinear Problems,
608 Including then-Way Parallel Factor Analysis Model, Journal of Computational and Graphical Statistics, 8, 854-888,
609 10.1080/10618600.1999.10474853, 1999.
610 Qin, Y. M., Tan, H. B., Li, Y. J., Schurman, M. I., Li, F., Canonaco, F., Prevot, A. S. H., and Chan, C. K.: Impacts of traffic
611 emissions on atmospheric particulate nitrate and organics at a downwind site on the periphery of Guangzhou,
612 China, Atmospheric Chemistry and Physics, 17, 10245-10258, 10.5194/acp-17-10245-2017, 2017.
613 Rollins, A. W., Browne, E. C., Min, K. E., Pusede, S. E., Wooldridge, P. J., Gentner, D. R., Goldstein, A. H., Liu, S., Day,
614 D. A., Russell, L. M., and Cohen, R. C.: Evidence for NO$_x$ Control over
615 Nighttime SOA Formation, Science, 337, 1210, 10.1126/science.1221520, 2012.
616 Sun, Y., Du, W., Fu, P., Wang, Q., Li, J., Ge, X., Zhang, Q., Zhu, C., Ren, L., Xu, W., Zhao, J., Han, T., Worsnop, D. R.,
617 and Wang, Z.: Primary and secondary aerosols in Beijing in winter: sources, variations and
618 processes, Atmospheric Chemistry and Physics, 16, 8309-8329, 10.5194/acp-16-8309-2016, 2016.
619 Sun, Y. L., Zhang, Q., Schwab, J. J., Demerjian, K. L., Chen, W. N., Bae, M. S., Hung, H. M., Hogrefe, O., Frank, B.,
620 Rattigan, O. V., and Lin, Y. C.: Characterization of the sources and processes of organic and inorganic aerosols in
621 New York city with a high-resolution time-of-flight aerosol mass apectrometer, Atmospheric Chemistry and Physics,
622 11, 1581-1602, 10.5194/acp-11-1581-2011, 2011.
623 Sun, Y. L., Wang, Z. F., Dong, H. B., Yang, T., Li, J., Pan, X. L., Chen, P., and Jayne, J. T.: Characterization of summer
624 organic and inorganic aerosols in Beijing, China with an Aerosol Chemical Speciation Monitor, Atmos. Environ., 51,
625 250-259, 10.1016/j.atmosenv.2012.01.013, 2012.
626 Sun, Y. L., Wang, Z. F., Fu, P. Q., Yang, T., Jiang, Q., Dong, H. B., Li, J., and Jia, J. J.: Aerosol composition, sources and
627 processes during wintertime in Beijing, China, Atmospheric Chemistry and Physics, 13, 4577-4592, 10.5194/acp-
628 13-4577-2013, 2013.
629 Sun, Y. L., Jiang, Q., Wang, Z. F., Fu, P. Q., Li, J., Yang, T., and Yin, Y.: Investigation of the sources and evolution
630 processes of severe haze pollution in Beijing in January 2013, J Geophys Res-Atmos, 119, 4380-4398,
631 10.1002/2014jd021641, 2014.

632   Sun, Y. L., Wang, Z. F., Du, W., Zhang, Q., Wang, Q. Q., Fu, P. Q., Pan, X. L., Li, J., Jayne, J., and Worsnop, D. R.: Long-
633   term real-time measurements of aerosol particle composition in Beijing, China: seasonal variations, meteorological
634   effects, and source analysis, Atmospheric Chemistry and Physics, 15, 10149-10165, 10.5194/acp-15-10149-2015,
635   2015.
636   Sun, Y. L., Xu, W. Q., Zhang, Q., Jiang, Q., Canonaco, F., Preevot, A. S. H., Fu, P. Q., Li, J., Jayne, J., Worsnop, D. R.,
637   and Wang, Z. F.: Source apportionment of organic aerosol from 2-year highly time-resolved measurements by an
638   aerosol chemical speciation monitor in Beijing, China, Atmospheric Chemistry and Physics, 18, 8469-8489,
639   10.5194/acp-18-8469-2018, 2018.
640   Ulbrich, I. M., Canagaratna, M. R., Zhang, Q., Worsnop, D. R., and Jimenez, J. L.: Interpretation of organic
641   components from Positive Matrix Factorization of aerosol mass spectrometric data, Atmospheric Chemistry and
642   Physics, 9, 2891-2918, 10.5194/acp-9-2891-2009, 2009.
643   Via, M., Minguillón, M. C., Reche, C., Querol, X., and Alastuey, A.: Increase in secondary organic aerosol in an urban
644   environment, Atmospheric Chemistry and Physics, 21, 8323-8339, 10.5194/acp-21-8323-2021, 2021.
645   Xu, L., Guo, H., Boyd, C. M., Klein, M., Bougiatioti, A., Cerully, K. M., Hite, J. R., Isaacman-VanWertz, G., Kreisberg, N.
646   M., Knote, C., Olson, K., Koss, A., Goldstein, A. H., Hering, S. V., de Gouw, J., Baumann, K., Lee, S. H., Nenes, A.,
647   Weber, R. J., and Ng, N. L.: Effects of anthropogenic emissions on aerosol formation from isoprene and
648   monoterpenes in the southeastern United States, Proc Natl Acad Sci U S A, 112, 37-42, 10.1073/pnas.1417609112,
649   2015a.
650   Xu, L., Suresh, S., Guo, H., Weber, R. J., and Ng, N. L.: Aerosol characterization over the southeastern United States
651   using high-resolution aerosol mass spectrometry: spatial and seasonal variation of aerosol composition and sources
652   with a focus on organic nitrates, Atmos. Chem. Phys., 15, 7307-7336, 10.5194/acp-15-7307-2015, 2015b.
653   Xu, W., Kuang, Y., Bian, Y., Liu, L., Li, F., Wang, Y., Xue, B., Luo, B., Huang, S., Yuan, B., Zhao, P., and Shao, M.: Current
654   Challenges in Visibility Improvement in Southern China, Environmental Science & Technology Letters, 7, 395-401,
655   10.1021/acs.estlett.0c00274, 2020.
656   Xu, W., Takeuchi, M., Chen, C., Qiu, Y., Xie, C., Xu, W., Ma, N., Worsnop, D. R., Ng, N. L., and Sun, Y.: Estimation of
657   particulate organic nitrates from thermodenuder–aerosol mass spectrometer measurements in the North China
658   Plain, Atmos. Meas. Tech., 14, 3693-3705, 10.5194/amt-14-3693-2021, 2021.
659   Yang, S., Yuan, B., Peng, Y., Huang, S., Chen, W., Hu, W., Pei, C., Zhou, J., Parrish, D. D., Wang, W., He, X., Cheng, C.,
660   Li, X. B., Yang, X., Song, Y., Wang, H., Qi, J., Wang, B., Wang, C., Wang, C., Wang, Z., Li, T., Zheng, E., Wang, S., Wu,
661   C., Cai, M., Ye, C., Song, W., Cheng, P., Chen, D., Wang, X., Zhang, Z., Wang, X., Zheng, J., and Shao, M.: The
662   formation and mitigation of nitrate pollution: comparison between urban and suburban environments, Atmos.
663   Chem. Phys., 22, 4539-4556, 10.5194/acp-22-4539-2022, 2022.
664   Yao, T., Li, Y., Gao, J., Fung, J. C. H., Wang, S., Li, Y., Chan, C. K., and Lau, A. K. H.: Source apportionment of secondary
665   organic aerosols in the Pearl River Delta region: Contribution from the oxidation of semi-volatile and intermediate
666   volatility primary organic aerosols, Atmospheric Environment, 222, 117111, 10.1016/j.atmosenv.2019.117111, 2020.
667   Yu, Y., Cheng, P., Li, H., Yang, W., Han, B., Song, W., Hu, W., Wang, X., Yuan, B., Shao, M., Huang, Z., Li, Z., Zheng, J.,
668   Wang, H., and Yu, X.: Budget of nitrous acid (HONO) at an urban site in the fall season of Guangzhou, China, Atmos.
669   Chem. Phys., 22, 8951-8971, 10.5194/acp-22-8951-2022, 2022.
670   Zhang, Q., Jimenez, J. L., Canagaratna, M. R., Allan, J. D., Coe, H., Ulbrich, I., Alfarra, M. R., Takami, A., Middlebrook,
671   A. M., Sun, Y. L., Dzepina, K., Dunlea, E., Docherty, K., DeCarlo, P. F., Salcedo, D., Onasch, T., Jayne, J. T., Miyoshi, T.,
672   Shimono, A., Hatakeyama, S., Takegawa, N., Kondo, Y., Schneider, J., Drewnick, F., Borrmann, S., Weimer, S.,
673   Demerjian, K., Williams, P., Bower, K., Bahreini, R., Cottrell, L., Griffin, R. J., Rautiainen, J., Sun, J. Y., Zhang, Y. M., and
674   Worsnop, D. R.: Ubiquity and dominance of oxygenated species in organic aerosols in anthropogenically-influenced
675   Northern Hemisphere midlatitudes, Geophysical Research Letters, 34, n/a-n/a, 10.1029/2007GL029979, 2007.

Atmospheric
Chemistry
and Physics
Discussions

676 Zhang, Q., Jimenez, J. L., Canagaratna, M. R., Ulbrich, I. M., Ng, N. L., Worsnop, D. R., and Sun, Y.: Understanding
677 atmospheric organic aerosols via factor analysis of aerosol mass spectrometry: a review, Analytical and Bioanalytical
678 Chemistry, 401, 3045-3067, 10.1007/s00216-011-5355-y, 2011.
679 Zhang, Y., Sun, J., Zhang, X., Shen, X., Wang, T., and Qin, M.: Seasonal characterization of components and size
680 distributions for submicron aerosols in Beijing, Science China Earth Sciences, 56, 890-900, 10.1007/s11430-012-
681 4515-z, 2012.
682 Zhang, Y. J., Tang, L. L., Wang, Z., Yu, H. X., Sun, Y. L., Liu, D., Qin, W., Canonaco, F., Prevot, A. S. H., Zhang, H. L.,
683 and Zhou, H. C.: Insights into characteristics, sources, and evolution of submicron aerosols during harvest seasons
684 in the Yangtze River delta region, China, Atmospheric Chemistry and Physics, 15, 1331-1349, 10.5194/acp-15-
685 1331-2015, 2015.
686 Zhou, W., Xu, W., Kim, H., Zhang, Q., Fu, P., Worsnop, D. R., and Sun, Y.: A review of aerosol chemistry in Asia:
687 insights from aerosol mass spectrometer measurements, Environ Sci Process Impacts, 22, 1616-1653,
688 10.1039/d0em00212g, 2020.
689